

Explaining Jupiter's magnetic field and equatorial jet dynamics

T. Gastine,¹ J. Wicht,¹ L. D. V. Duarte,^{1,2} M. Heimpel³, and A. Becker⁴

Spacecraft data reveal a very Earth-like Jovian magnetic field [Connerney *et al.*, 1998; Connerney, 2007]. This is surprising since numerical simulations have shown that the vastly different interiors of terrestrial and gas planets can strongly affect the internal dynamo process. Here we present the first numerical dynamo that manages to match the structure and strength of the observed magnetic field by embracing the newest models for Jupiter's interior [Nettelmann *et al.*, 2012; French *et al.*, 2012]. Simulated dynamo action primarily occurs in the deep high electrical conductivity region while zonal flows are dynamically constrained to a strong equatorial jet in the outer envelope of low conductivity. Our model reproduces the structure and strength of the observed global magnetic field and predicts that secondary dynamo action associated to the equatorial jet produces banded magnetic features likely observable by the Juno mission. Secular variation in our model scales to about 2000 nT per year and should also be observable during the one year nominal mission duration.

1. Introduction

Spacecraft data allow to model the Jovian magnetic field up to spherical harmonic degree and order 4 – 5 [Connerney *et al.*, 1998; Connerney, 2007; Hess *et al.*, 2011]. The observations reveal that the Jovian magnetic field is dominated by a tilted dipole with an Earth-like inclination angle around 10° and is about an order of magnitude stronger than the geomagnetic field. Tracking cloud features with ground-based and space observations show that the Jovian surface dynamics is dominated by strong zonal motions of unknown and highly debated depth. These zonal winds form a differential rotation profile with alternating prograde (i.e. eastward) and retrograde (westward) flows [e.g. Porco *et al.*, 2003].

Jupiter's atmosphere mainly consists of hydrogen and helium (roughly a quarter by mass), surrounding a rocky inner core with a radius likely less than 10% of Jupiter's mean radius R_J (1 bar level) [Nettelmann *et al.*, 2012]. Laboratory experiments and ab initio simulations have shown that hydrogen undergoes a phase transition from a molecular to a metallic state at increasing pressure and temperature [Nellis *et al.*, 1995; French *et al.*, 2012]. The Jovian dynamo is thought to operate below a transition radius, located

between 0.85 and 0.90 R_J , while the observed fierce zonal winds likely dominate the dynamic of the outer molecular layer. Increasing density, Lorentz forces and Ohmic dissipation would lead to slower fluid velocities in the metallic layer and confine the zonal winds to the upper region [e.g. Liu *et al.*, 2008]. Classical dynamical models therefore treat the dynamics of these two layers separately, focussing either on the dynamo action [Christensen and Aubert, 2006; Gastine *et al.*, 2012] or on the zonal winds driving [Heimpel *et al.*, 2005; Jones and Kuzanyan, 2009; Kaspi *et al.*, 2009; Gastine and Wicht, 2012; Gastine *et al.*, 2014]. However, since electrical conductivity and density increase continuously with depth throughout the transition [Lorenzen *et al.*, 2011; French *et al.*, 2012], as illustrated in Fig. 1, the coupling between both layers may actually be significant. Stanley and Glatzmaier [2010] incorporate both the density and the electrical conductivity variations but only simulate the dynamics in the very outer envelope where the conductivity decays exponentially. They report multiple zonal jets but the magnetic field is too axisymmetric, too little dipolar, and too concentrated at higher latitudes. The model by Heimpel and Gómez Pérez [2011] spans the metallic and the molecular envelope but ignores the density variation. They only find dipole dominated solutions close to the onset of dynamo action where the field structure and dynamics is too simplistic. The approach by Duarte *et al.* [2013] is very similar to the model presented here but the density profile follows an ideal equation of state and the electrical conductivity only drops by two orders of magnitude over the simulated shell. Once more, dipole-dominated solutions are restricted to low Rayleigh numbers where the overall dynamics remains too simple.

Here, we present a numerical simulation that models the density contrast up to 99% of the Jupiter's radius (1 bar level) and uses a more realistic electrical conductivity profile that mimics the severe drop over the molecular layer. The good agreement of the large scale field with current magnetic field models indicates that the model provides useful constraints for the Juno spacecraft, which is scheduled to arrive at Jupiter in august 2016.

2. Dynamo Model

We consider convection and dynamo action in a spherical shell rotating at a constant rate Ω about the z -axis. The numerical MHD code MagIC uses pseudospectral methods and a mixed implicit/explicit time-stepping scheme to solve for the Navier-Stokes equation, the induction equation, and the entropy equation [Christensen and Wicht, 2007]. We adopt an anelastic approach [Lantz and Fan, 1999; Jones *et al.*, 2011] to include a background density profile $\bar{\rho}$ that represents a seventh order polynomial fit to the ab initio predictions [French *et al.*, 2012]. The background temperature \bar{T} is then approximated by a polytropic equation of state of the form $\bar{T} = \bar{\rho}^{1/m}$, where $1/m = 0.45$. Modelling Jupiter's large density contrast illustrated in Fig. 1a is computationally challenging. By using a fine spatial grid we could afford to model the dynamics up to 99% of Jupiter's radius, closely following the predicted profile. The inner 19.8% in radius are occupied by a solid electrically conducting inner core.

¹Max-Planck-Institut für Sonnensystemforschung, Justus-von-Liebig-Weg 3, 37077 Göttingen, Germany.

²Laboratoire de Géologie de Lyon, CNRS, Université de Lyon, France.

³Department of Physics, University of Alberta, Edmonton, Alberta T6G 2J1, Canada.

⁴Institut für Physik, Universität Rostock, 18051 Rostock, Germany.

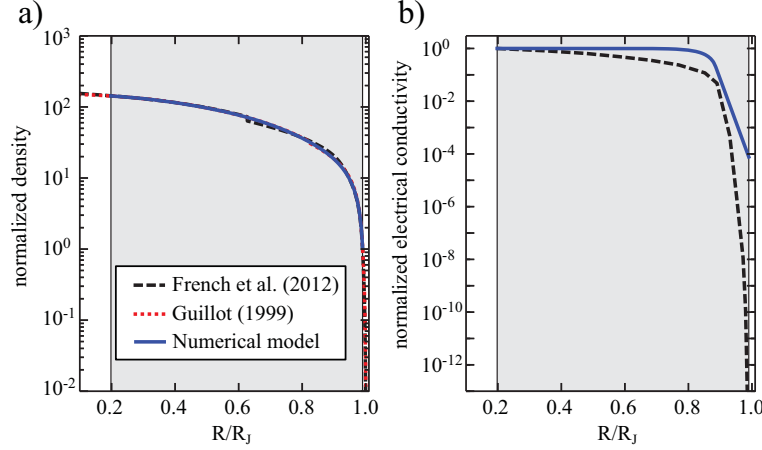


Figure 1. Comparison of the density (panel a) and electrical conductivity profile (panel b) used in the numerical simulation with interior models for Jupiter [Guillot, 1999; French et al., 2012]. The density has been normalized with the reference value at $0.99 R_J$, while the electrical conductivity has been normalized with the reference value at $0.2 R_J$. These radii represent the outer and inner boundary in the numerical model (blue line).

Adopting a conducting inner core eases the comparison with previous numerical calculations [Duarte et al., 2013]. The actual size and thermodynamic properties of Jupiter's core are still a matter of debate [Nettelmann et al., 2012; Cebulla and Redmer, 2014]. However, since the inner core in our numerical model is small the effects of its conductivity are likely negligible [Schubert and Zhang, 2001; Wicht, 2002]. The density increases by a factor of 137 over the simulated shell, which corresponds to 4.92 density scale heights. The density drops by an additional factor of 174 over the last outer 1% in radius. Resolving this severe gradient numerically would be extremely costly.

The electrical conductivity profile predicted by ab initio simulations (Fig. 1b) indicates a continuous transition from the molecular to the metallic state with a clear change in slope where the hydrogen molecules become completely dissociated. While the conductivity increases only mildly with radius at depth, the gradient quickly becomes super-exponential beyond $0.9 R_J$. Resolving this steep decrease poses additional numerical problems. As a compromise, we assume that the conductivity remains constant in the deeper interior and decreases exponentially by four orders of magnitude beyond the transition radius $0.87 r_o$ where r_o is the outer radius in the simulation [Gómez-Pérez et al., 2010; Duarte et al., 2013]. This choice is motivated by the magnetic Reynolds number profile further discussed below.

The dimensionless anelastic equations solved by MagIC are governed by four dimensionless numbers: the Ekman number $E = \nu/\Omega d^2$; the modified Rayleigh number $Ra^* = T_o \Delta s / \Omega^2 d^2$; the Prandtl number $Pr = \nu/\kappa$; and the magnetic Prandtl number $Pm = \nu/\lambda(r_i)$. These parameters combine characteristic physical properties of the system: the rotation rate Ω , the shell thickness d , the temperature at the outer boundary T_o , the entropy contrast over the shell Δs , the kinematic viscosity ν , the thermal diffusivity κ , and the magnetic diffusivity at the inner boundary $\lambda(r_i)$. Stress-free mechanical boundary conditions are used at the outer boundary while rigid conditions model the interface to the conducting inner core. The magnetic field matches a diffusive solution at the inner boundary and a potential field at the outer boundary. Convection is driven with an imposed constant entropy contrast over the shell. Although internal heating would be more realistic for Jupiter's heating mode, some preliminary numerical simulations with internal heating at $E = 10^{-4}$ yield very similar solutions as the cases

without. This suggests that the shape of the convective pattern is primarily controlled by the local buoyancy variations caused by the density contrast while the distribution of buoyancy sources plays a secondary role. However, further parameter studies will be needed to systematically check the influence of internal heating on rotating compressible convection.

Starting with an Ekman number of $E = 10^{-4}$ and a magnetic Prandtl number of $Pm = 2$ we lowered these values gradually down to $E = 10^{-5}$ and $Pm = 0.6$. The final setup was integrated for 0.3 magnetic diffusion times. The Prandtl number has been fixed to $Pr = 1$ and the Rayleigh number of $Ra^* = 6.16 \times 10^{-3}$ has been chosen to obtain strongly-driven convective motions and a complex enough yet still dipole-dominated magnetic field [Duarte et al., 2013].

The spatial resolution of this numerical model is defined by the maximum spherical harmonic degree ($\ell_{max} = 426$) and the number of radial levels ($N_r = 145$).

3. Rescaling to Physical Units

Due to numerical limitations it remains impossible to choose realistic values for all the physical properties in a direct numerical simulation. The Ekman number is $E = 10^{-5}$ and the magnetic Prandtl number $Pm = 0.6$ in our dynamo model where values around $E = 10^{-18} - 10^{-19}$ and $Pm = 10^{-7}$ would be appropriate for Jupiter. Boussinesq and anelastic dynamo models computed in the accessible range $E \in [10^{-6} - 10^{-3}]$ suggested that the rms field magnetic field strength and rms convective flow amplitude in the simulated shell depend on the available power. The respective scaling laws predict reasonable values for planets or fully convective stars [Christensen and Aubert, 2006; Christensen, 2010] and can be used to extrapolate the numerical results. Our model obeys the anelastic scaling laws [Yadav et al., 2013] for the dimensionless rms flow amplitude

$$U^* = 1.65 P^{*0.42}, \quad (1)$$

where $P^* = P/(\Omega^3 d^2)$ is the dimensionless form of the convective power per unit mass P . The dimensionless rms magnetic field strength B^* has been found to scale like

$$B^* = \sqrt{f_{Ohm} \rho^*} P^{*0.35}. \quad (2)$$

The factor f_{Ohm} is the ratio of Ohmic to viscous dissipation and is close to one for planetary dynamo regions where the

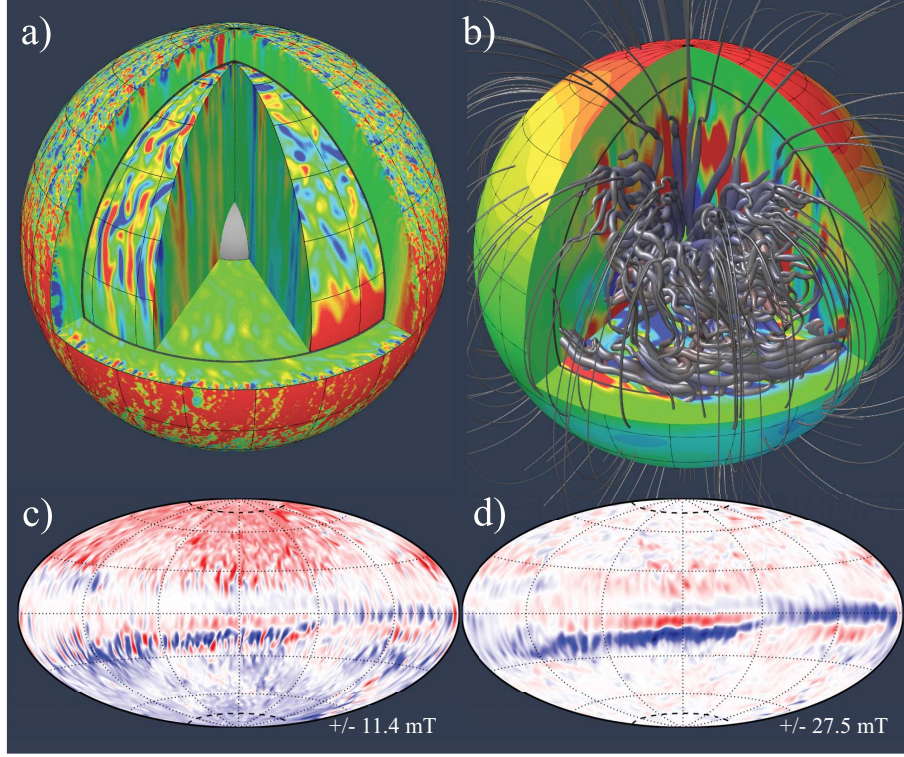


Figure 2. Panel a) shows the azimuthal flow component on the outer surface and the right cut while the radial flow component is shown in the equatorial and left cuts. The inset sphere slices visualize the weaker flow at greater depths. The right inset shows the azimuthal flow amplified by a factor 10 and the left inset shows the radial flow amplified by a factor 2.5. The flow amplitude strongly increases with radius while the length scale decreases. Panel b) shows the radial magnetic field on the outer surface and the left cut. The surface field has been amplified by a factor 10. The right and horizontal cuts (at -10°) show the azimuthal magnetic field. The thickness of the magnetic fieldlines has been scaled with the third root of the local magnetic field strength. Panels c) and d) show the radial and azimuthal magnetic field at the transition radius $0.87 r_o$ that is marked with a dark grey line in panels a) and b). Yellow/red (blue) indicates outward (inward) or eastward (westward) directions.

magnetic diffusivity is orders of magnitude larger than the viscous diffusivity. ρ^* is the mean dimensionless density.

The available convective power can be estimated based on the net heat flux density F out of a planetary dynamo region [Christensen, 2010]. Using the Jovian net heat flux $F_J = 5.5 \text{ W/m}^2$ [e.g. Hanel *et al.*, 1981], $M_J = 1.83 \times 10^{27} \text{ kg}$ and $R_J = 6.99 \times 10^4 \text{ km}$ and the radial profiles by French *et al.* [2012] for the heat capacity c_p , gravity g and thermal expansivity α yields

$$P = \frac{4\pi R_J^2 F_J}{M_J} \int \frac{\alpha g}{c_p} dr \approx 4.6 \times 10^{-10} \text{ W/kg} . \quad (3)$$

Eq. (1) then provides an estimate for the dimensionless rms flow speed which can be converted into a dimensional value using Jupiter's rotation rate $\Omega = 1.75 \times 10^{-4} \text{ s}^{-1}$ and shell thickness $d = (0.99 - 0.2)R_J = 5.52 \times 10^4 \text{ km}$:

$$U_J = U_J^* \Omega d \approx 3 \text{ cm/s} . \quad (4)$$

Following the same procedure but using Eq. (2), the mean Jovian density $\rho_J = 1300 \text{ kg/m}^3$ and the magnetic permeability μ predicts Jupiter's rms magnetic field strength:

$$B_J = B_J^* \Omega d (\rho_J \mu)^{1/2} \approx 7 \text{ mT} . \quad (5)$$

Both values reasonably agree with estimates for Jupiter which seems to confirm the applicability of these scaling laws [Christensen and Aubert, 2006].

Since our simulation closely follows the scaling laws we can simply rescale the result by assuming that the dimen-

sionless rms flow and magnetic field amplitudes are identical to U_J and B_J respectively. The flow velocity also allows to estimate Jupiter's typical convective time scale $t_c = d/U = 53 \text{ yr}$, often referred to as the turnover time. To predict the time variability of the Jovian magnetic field we have assumed that the convective overturn time in our simulation agrees with the respective Jovian value. This scaling implies that the simulation covers roughly 6500 yr.

4. Results and Implications for Jupiter

Fig. 2 illustrates the flow and magnetic field generation in our numerical model. Owing to the strong density stratification, the length scale of the non-zonal convective flow decreases with radius while the amplitude increases [see equatorial cut in Fig. 2a and Gastine and Wicht, 2012]. These convective motions maintain a prograde equatorial zonal flow via Reynolds stresses [see right cut in Fig. 2a and Heimpel *et al.*, 2005]. Lorentz forces constrain the equatorial jet to the weakly conducting outer envelope and largely suppress flanking higher latitude jets [Duarte *et al.*, 2013].

The magnetic Reynolds number $Rm = U d \mu \sigma$ measures the ratio of magnetic field production to Ohmic dissipation and is thus an important quantity for any dynamo process. Here, U is a typical flow velocity, μ the magnetic permeability, σ the electrical conductivity, and d the depth of the simulated spherical shell. Numerical simulations suggest that Rm must typically exceed 50 to guarantee dynamo action [Christensen and Aubert, 2006]. In the model presented here, Rm assumes a complex radial profile since U

increases with radius while σ decreases. Rm reaches a peak value around 220 in the inner conducting layer, decreases to $Rm = 50$ near $r = 0.9r_o$, and reaches $Rm = 0.2$ at the outer boundary. The combination of the mean flow velocity U and the electrical conductivity profile thus guarantees no dynamo action in the very outer envelope but leaves room for induction effects in the transitional zone.

Fig. 2 indeed demonstrates that the primary dipole-dominated magnetic field is created at depth where Rm is significant, the electrical conductivity high, and the density contrast relatively mild. A secondary dynamo mechanism operates at low latitudes and slightly below the transition radius where Rm is still sufficient for dynamo action. Here, the remaining zonal shear (right inner sphere in Fig. 2a) creates a strong azimuthal magnetic field. At the transition region, the magnetic banding (Fig. 2d) associated with the shear of the equatorial jet is reminiscent to the so-called “wreaths of magnetism” found in the solar dynamo models by *Brown et al.* [2010]. The non-zonal convective motions convert this azimuthal field into banded radial field structures (see thick horizontal fieldlines in Fig. 2b and radial magnetic field at the transition radius in Fig. 2c).

The inhibition of dynamo action in the very outer envelope is essential since previous numerical models have shown that the vigorous small scale flows and the strong equatorial jet located in this layer would promote multipolar magnetic fields [*Gastine et al.*, 2012; *Duarte et al.*, 2013]. In our model, the decrease in electrical conductivity is not as steep as suggested by the ab initio simulations but still sufficient to compensate for the radial increase in flow amplitude. It is also steeper than in previous simulations [*Duarte et al.*, 2013] which allowed us to adopt a larger Rayleigh number. While this promotes a more vigorous and dynamic convection, the lower conductivity in the very outer shell guarantees that this region plays no role in the dynamo process. This not only promotes a more vigorous flow but also a more complex and time dependent solution that is much closer to Jupiter's magnetic field. At lower Rayleigh numbers for example the axial dipole component is much too dominant, as in the dynamo models by *Heimpel and Gómez Pérez* [2011].

Estimates for Jupiter predict a much larger magnetic Reynolds number (7×10^5 using Eq. 1) than in our model. Increasing the mean Rm in the simulation would require a yet steeper electrical conductivity profile to minimize dynamo action in the molecular layer. Additionally, smaller viscosities may have to be adopted to retain dipole-dominated dynamo action [*Christensen and Aubert*, 2006; *Duarte et al.*, 2013]. Though suggested by the ab initio simulations, both of these measures are currently too expensive for numerical resources.

Jupiter's surface dynamics is dominated by a system of banded strong zonal winds where the dominant equatorial jet is flanked by several secondary jets at higher latitudes. These secondary jets are not captured by our simulation. Previous studies suggest that a smaller viscosity help to promote the secondary jets in numerical simulations [*Jones and Kuzanyan*, 2009; *Gastine et al.*, 2014]. However, the dynamo action of deeper reaching zonal winds may lead to a magnetic field geometry that is not very Jupiter-like [*Gastine et al.*, 2012; *Duarte et al.*, 2013; *Stanley and Glatzmaier*, 2010]. The strong azimuthal magnetic fields likely produced by deeper reaching zonal winds would also cause a thermal Ohmic dissipation signal which has not been detected [*Liu et al.*, 2008, 2013]. However, Ohmic heating is not expected to be strong for the dominant equatorial jet which remains confined to the weakly conducting outer envelope. Some authors predict that the secondary jets remain restricted to Jupiter's weather layer not represented in our model [*Kaspi et al.*, 2009]. The gravity signal measured by the Juno mission will provide additional constraints on the depth of the Jovian zonal winds [*Kaspi*, 2013; *Liu et al.*, 2013].

Fig. 3 and Fig. 4 compare the magnetic field in our simulation with models of Jupiter's magnetic field. The Jovian magnetic field has been measured by several space missions but since data taken below the magnetospheric stand-off distance remain scarce only the large scale field can be constrained. Observations of Io's auroral footprint provide some additional information [*Connerney et al.*, 1998; *Hess et al.*, 2011]. Global magnetic fields are commonly decomposed into spherical harmonic contributions with the Gauss coefficients $g_{\ell m}$ and $h_{\ell m}$ describing the internal magnetic field of spherical harmonic degree ℓ and order m at planetary surface [*Chapman and Bartels*, 1940]. The magnetic

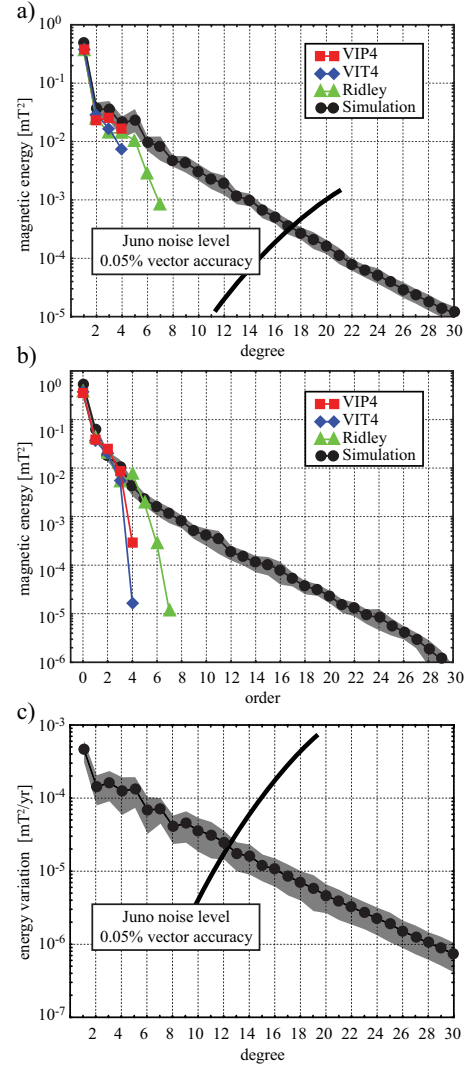


Figure 3. Panel a) and b) show a comparison of the magnetic energy spectra per spherical harmonic degree ℓ and order m for the three different Jupiter field models VIP4 [*Connerney et al.*, 1998], VIT4 [*Connerney*, 2007] and Ridley [*Ridley*, 2012] with the time averaged spectrum of the numerical simulation. The thick black lines in panel a) illustrate the predicted noise level for the Juno magnetometer. Panel c) shows the time averaged absolute variation in the ℓ energy spectrum per year for the numerical simulation. The grey bar around the simulated spectra has the width of the standard deviation and provides an idea of the time dependence. The thick curved black lines in panels a) and c) illustrate an estimate for the Juno noise level assuming that the magnetometer delivers the conservatively expected 0.05% vector accuracy. The secular variation noise level will be somewhat higher than indicated in panel c) since this estimate assumes that all the data acquired during the nominal one year mission duration are used.

energy $W_{\ell m}$ carried by the pair $g_{\ell m}$ and $h_{\ell m}$ then provides the energy for a specific degree and order:

$$W_{\ell m} = (\ell + 1) (g_{\ell m}^2 + h_{\ell m}^2). \quad (6)$$

The energy spectrum per spherical harmonic degree or order can then be calculated by summing the respective contribu-

tions:

$$W_{\ell} = \sum_{m=0}^{\ell} (\ell + 1) (g_{\ell m}^2 + h_{\ell m}^2), \quad (7)$$

$$W_m = \sum_{\ell=m}^{\ell=L} (\ell + 1) (g_{\ell m}^2 + h_{\ell m}^2), \quad (8)$$

where L is the truncation degree of the model. Fig. 3a and b compare the magnetic energy spectra of three Jupiter field models with the time averaged spectra from our numerical simulation. The Jupiter models VIP4 and VIT4 cover contributions up to $\ell = 4$ while the Ridley model reaches up to $\ell = 7$. The disagreement between the different models indicates that the data are not sufficient to uniquely constrain degrees beyond $\ell = 2$. The regularization strongly affects degree $\ell = 4$ contributions in VIP4 and VIT4 and $\ell = 5$ and $\ell = 6$ in the Ridley model. The rescaled numerical simulation predicts a mean magnetic field strength that is about 40% stronger than the observation, a very reasonable agreement considering the model limitations. The shape of the spectra agrees nicely with the field models.

To estimate the secular variation, we calculate the time averaged spectral variation per year:

$$\langle \dot{w}_{\ell} \rangle = \langle |W_{\ell}(t + \delta t) - W_{\ell}(t)| / \delta t \rangle \quad (9)$$

where the triangular brackets denote the time average. The respective spectrum is shown in Fig. 3c. The variation amounts to about 0.1% at $\ell = 1$ and reaches a level of 0.01% of the dipole energy at $\ell = 10$. The high precision level of the Juno magnetometer should allow to detect such a secular variation signal in at least the small ℓ contributions (J. Connerney, private communication). Note however that the noise level shown in Fig. 3c assumes data compiled over the nominal one year mission duration. The true secular variation noise level will thus be higher.

Fig. 4 compares the magnetic field for a selected snapshot of the simulation with the VIP4 internal field model [Connerney *et al.*, 1998]. The overall field structure up to spherical harmonic degree $\ell = 4$ is very well captured by the numerical model. The dipole tilt for the snapshot ($\Theta = 6^\circ$) is somewhat lower than that for Jupiter ($\Theta = 10.1^\circ$) but changes constantly over the simulation with an average rate of 0.02 degree per year. The mean tilt is $\Theta = 7.5^\circ$ and it reaches a maximum of $\Theta = 18.5^\circ$. The rms surface field strength also varies significantly around the mean value of 0.39 mT and can double over a time span of about 500 yr. The mean rate of change is somewhat slower at 0.1% per year. Both the variation in tilt and field strength are consistent with observations [Russell *et al.*, 2001; Ridley, 2012].

A comparison of the radial magnetic field at the transition radius (Fig. 2c) and at the surface of the simulation (Fig. 4d) demonstrates that the higher harmonics decrease rapidly over the weakly conducting outer envelope. However, the azimuthally extended bands remain a clearly identifiable surface manifestation of the deeper dynamo action associated to the equatorial jet.

A primary goal of the Juno mission is to significantly increase the knowledge of the Jovian magnetic field. The spacecraft is scheduled to orbit Jupiter 30 times during its one year nominal mission duration. The first 15 orbits are separated by 24° in longitude so that a global but somewhat coarse coverage is achieved after half the mission duration. The following 15 orbits are shifted by 12° in longitude to the first set. The noise estimate shown in Fig. 3 assumes that the magnetometer delivers a vector accuracy of 0.05%

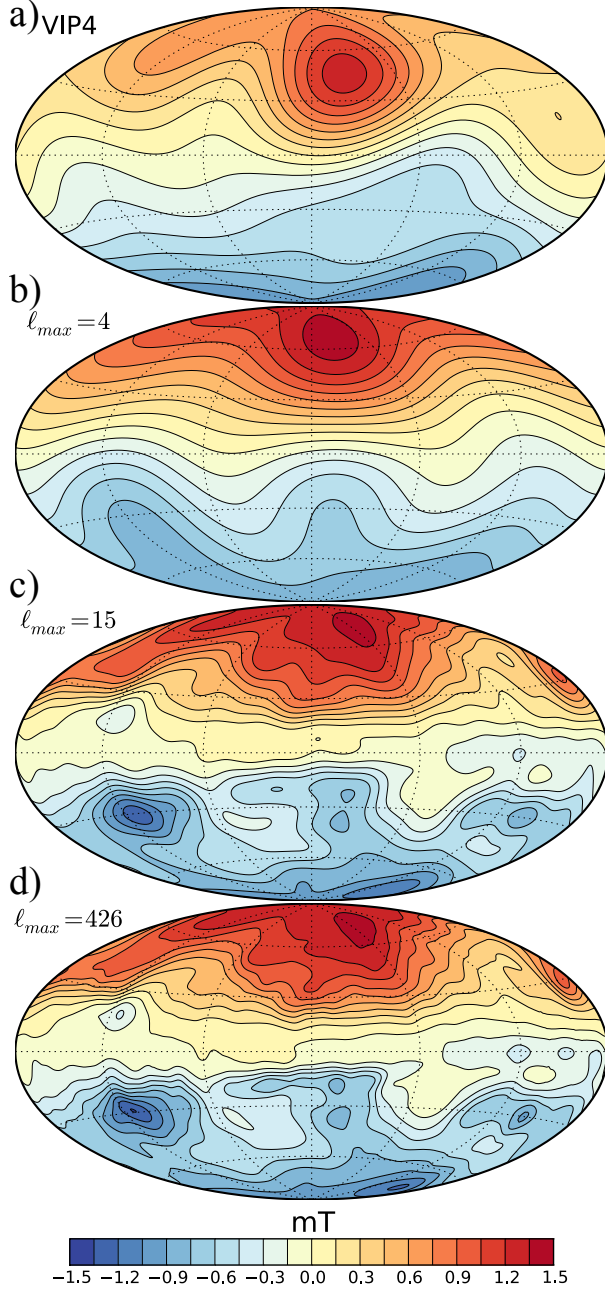


Figure 4. Comparison of the radial surface field of the Jupiter field model VIP4 [Connerney *et al.*, 1998] in panel a) with a selected snapshot from the numerical simulation shown at three different spherical harmonic resolutions. Panel b) depicts the same maximum spherical harmonic resolution $\ell_{max} = 4$ as VIP4, panel c) illustrates the field at $\ell_{max} = 15$, close to the expected Juno detection limit, while panel d) shows the full numerical solution with $\ell_{max} = 426$.

which is in part limited by attitude information from the spacecraft's star camera. However, the unique co-location of magnetometer and star camera at the end of one of the three solar panels may allow an even higher accuracy. The noise estimate furthermore assumes that external field contributions can be modelled to an equivalent error level and that data points separated by one minute flight time have uncorrelated errors and can thus be used as independent data. The error propagation into the field model is calculated for a standard least square fit of the data to the spherical harmonic representation via Gauss coefficients (J. Connerney, private communication). This predicts that Juno data will constrain the field up to $\ell = 18$ or better. Fig. 4 demonstrates that for our simulation basically all the magnetic field features are already captured at degree 15. Furthermore magnetic banding due to the equatorial jet is at times more pronounced than shown in Fig. 2. Thus, our results indicate that the Juno mission will allow detection of the low latitude magnetic bands.

In conclusion, we present a numerical model for interior dynamics that incorporates up-to-date knowledge of Jupiter's interior and is the first to successfully reproduce the Jovian large scale magnetic field. Previous attempts to model Jupiter's interior dynamics have indeed largely failed to reproduce important features of the planet's large scale magnetic field. They were either too simplistic with a too strong dipolar component [Heimpel and Gómez Pérez, 2011; Duarte et al., 2013] or they were restricted to the outer envelope dynamics producing a too axisymmetric and too little dipolar magnetic field [Stanley and Glatzmaier, 2010]. Here, the combination of a deep-seated dipolar dynamo and a magnetic banding associated with the equatorial jet is a key feature that distinguishes our model from these previous numerical attempts. The predictions of the magnetic field morphology at global and regional scales, and of the secular variation, will allow our model to be tested against Juno measurements.

Acknowledgments. We thank J. Connerney for providing Juno's magnetometer specifications and T. Dannert for his development of the MPI version of the MagIC code. All the computations have been carried out on the IBM iDataPlex HPC System Hydra at the MPG Rechenzentrum Garching. TG and LD are supported by the Special Priority Program 1488 PlanetMag of the German Science Foundation. MH is supported in part by an NSERC Discovery Grant.

References

- Brown, B. P., M. K. Browning, A. S. Brun, M. S. Miesch, and J. Toomre (2010), Persistent Magnetic Wreaths in a Rapidly Rotating Sun, *ApJ*, *711*, 424–438, doi:10.1088/0004-637X/711/1/424.
- Cebulla, D., and R. Redmer (2014), Ab initio simulations of MgO under extreme conditions, *Phys. Rev. B*, *89*(13), 134107, doi:10.1103/PhysRevB.89.134107.
- Chapman, S., and J. Bartels (1940), *Geomagnetism*, Oxford Uni. Press, New York.
- Christensen, U. R. (2010), Dynamo Scaling Laws and Applications to the Planets, *Space Sci. Rev.*, *152*, 565–590, doi:10.1007/s11214-009-9553-2.
- Christensen, U. R., and J. Aubert (2006), Scaling properties of convection-driven dynamos in rotating spherical shells and application to planetary magnetic fields, *Geophysical Journal International*, *166*, 97–114, doi:10.1111/j.1365-246X.2006.03009.x.
- Christensen, U. R., and J. Wicht (2007), Numerical dynamo simulations, in *Treatise on Geophysics, Volume 8: Core Dynamics*, edited by G. Schubert, pp. 245–282, Elsevier, Amsterdam.
- Connerney, J. E. P. (2007), Planetary magnetism, in *Treatise on Geophysics, Vol. 20: Planets and Moons*, edited by G. Schubert, pp. 243–280, Elsevier, Amsterdam.
- Connerney, J. E. P., M. H. Acuña, N. F. Ness, and T. Satoh (1998), New models of Jupiter's magnetic field constrained by the Io flux tube footprint, *J. Geophys. Res.*, *103*, 11,929–11,940, doi:10.1029/97JA03726.
- Duarte, L. D. V., T. Gastine, and J. Wicht (2013), Anelastic dynamo models with variable electrical conductivity: An application to gas giants, *Physics of the Earth and Planetary Interiors*, *222*, 22–34, doi:10.1016/j.pepi.2013.06.010.
- French, M., A. Becker, W. Lorenzen, N. Nettelmann, M. Bethkenhagen, J. Wicht, and R. Redmer (2012), Ab Initio Simulations for Material Properties along the Jupiter Adiabats, *ApJS*, *202*, 5, doi:10.1088/0067-0049/202/1/5.
- Gastine, T., and J. Wicht (2012), Effects of compressibility on driving zonal flow in gas giants, *Icarus*, *219*, 428–442, doi:10.1016/j.icarus.2012.03.018.
- Gastine, T., L. Duarte, and J. Wicht (2012), Dipolar versus multipolar dynamos: the influence of the background density stratification, *A&A*, *546*, A19, doi:10.1051/0004-6361/201219799.
- Gastine, T., M. Heimpel, and J. Wicht (2014), Zonal flow scaling in rapidly-rotating compressible convection, *Physics of the Earth and Planetary Interiors*, *232*, 36–50, doi:10.1016/j.pepi.2014.03.011.
- Gómez-Pérez, N., M. Heimpel, and J. Wicht (2010), Effects of a radially varying electrical conductivity on 3D numerical dynamos, *Physics of the Earth and Planetary Interiors*, *181*, 42–53, doi:10.1016/j.pepi.2010.03.006.
- Guillot, T. (1999), Interior of Giant Planets Inside and Outside the Solar System, *Science*, *286*, 72–77, doi:10.1126/science.286.5437.72.
- Hanel, R., B. Conrath, L. Herath, V. Kunde, and J. Pirraglia (1981), Albedo, internal heat, and energy balance of Jupiter - Preliminary results of the Voyager infrared investigation, *J. Geophys. Res.*, *86*, 8705–8712.
- Heimpel, M., and N. Gómez Pérez (2011), On the relationship between zonal jets and dynamo action in giant planets, *Geophys. Res. Lett.*, *38*, L14,201, doi:10.1029/2011GL047562.
- Heimpel, M., J. Aurnou, and J. Wicht (2005), Simulation of equatorial and high-latitude jets on Jupiter in a deep convection model, *Nature*, *438*(10), 193–196, doi:10.1038/nature04208.
- Hess, S. L. G., B. Bonfond, P. Zarka, and D. Grodent (2011), Model of the Jovian magnetic field topology constrained by the Io auroral emissions, *J. Geophys. Res.*, *116*, A05217, doi:10.1029/2010JA016262.
- Jones, C. A., and K. M. Kuzanyan (2009), Compressible convection in the deep atmospheres of giant planets, *Icarus*, *204*, 227–238, doi:10.1016/j.icarus.2009.05.022.
- Jones, C. A., P. Boronski, A. S. Brun, G. A. Glatzmaier, T. Gastine, M. S. Miesch, and J. Wicht (2011), Anelastic convection-driven dynamo benchmarks, *Icarus*, *216*, 120–135, doi:10.1016/j.icarus.2011.08.014.
- Kaspi, Y. (2013), Inferring the depth of the zonal jets on Jupiter and Saturn from odd gravity harmonics, *Geophys. Res. Lett.*, *40*, 676–680, doi:10.1029/2012GL053873.
- Kaspi, Y., G. R. Flierl, and A. P. Showman (2009), The deep wind structure of the giant planets: Results from an anelastic general circulation model, *Icarus*, *202*, 525–542, doi:10.1016/j.icarus.2009.03.026.
- Lantz, S. R., and Y. Fan (1999), Anelastic magnetohydrodynamic equations for modeling solar and stellar convection zones, *ApJS*, *121*, 247–264.
- Liu, J., P. M. Goldreich, and D. J. Stevenson (2008), Constraints on deep-seated zonal winds inside Jupiter and Saturn, *Icarus*, *196*, 653–664, doi:10.1016/j.icarus.2007.11.036.
- Liu, J., T. Schneider, and Y. Kaspi (2013), Predictions of thermal and gravitational signals of Jupiter's deep zonal winds, *Icarus*, *224*, 114–125, doi:10.1016/j.icarus.2013.01.025.
- Lorenzen, W., B. Holst, and R. Redmer (2011), Metallization in hydrogen-helium mixtures, *Phys. Rev. B*, *84*(23), 235109, doi:10.1103/PhysRevB.84.235109.
- Nellis, W. J., M. Ross, and N. C. Holmes (1995), Temperature Measurements of Shock-Compressed Liquid Hydrogen: Implications for the Interior of Jupiter, *Science*, *269*, 1249–1252, doi:10.1126/science.7652570.

- Nettelmann, N., A. Becker, B. Holst, and R. Redmer (2012), Jupiter Models with Improved Ab Initio Hydrogen Equation of State (H-REOS.2), *ApJ*, *750*, 52, doi:10.1088/0004-637X/750/1/52.
- Porco, C. C., R. A. West, A. McEwen, A. D. Del Genio, A. P. Ingersoll, P. Thomas, S. Squyres, L. Dones, C. D. Murray, T. V. Johnson, J. A. Burns, A. Brahic, G. Neukum, J. Veverka, J. M. Barbara, T. Denk, M. Evans, J. J. Ferrier, P. Geissler, P. Helfenstein, T. Roatsch, H. Throop, M. Tiscareno, and A. R. Vasavada (2003), Cassini Imaging of Jupiter's Atmosphere, Satellites, and Rings, *Science*, *299*, 1541–1547, doi:10.1126/science.1079462.
- Ridley, V. A. (2012), Jovimagnetic secular variation, Ph.D. thesis, University of Liverpool, United Kingdom.
- Russell, C. T., Z. J. Yu, and M. G. Kivelson (2001), The rotation period of Jupiter, *Geophys. Res. Lett.*, *28*, 1911–1912, doi:10.1029/2001GL012917.
- Schubert, G., and K. Zhang (2001), Effects of an Electrically Conducting Inner Core on Planetary and Stellar Dynamos, *ApJ*, *557*, 930–942, doi:10.1086/321687.
- Stanley, S., and G. A. Glatzmaier (2010), Dynamo models for planets other than Earth, *Space Sci. Rev.*, *152*, 617–649, doi:10.1007/s11214-009-9573-y.
- Wicht, J. (2002), Inner-core conductivity in numerical dynamo simulations, *Physics of the Earth and Planetary Interiors*, *132*, 281–302.
- Yadav, R. K., T. Gastine, U. R. Christensen, and L. D. V. Duarte (2013), Consistent Scaling Laws in Anelastic Spherical Shell Dynamos, *ApJ*, *774*, 6, doi:10.1088/0004-637X/774/1/6.
-